A PERFORMANCE EVALUATION OF THE ARCH BRIDGE MEMBERS USING THE STRAIN INDEX BASED ON THE PARAMETERS OBTAINED FROM LINEAR BUCKLING THEORY

Sujaritpong Atavit[1,*] and Toshitaka Yamao[2]

[1]*Graduate School of Science and Technology, Kumamoto University, 2-39-1 Kurokami, Kumamoto 860-8555, Japan*
[2]*Department of Civil Engineering and Architectures, Kumamoto University, 2-39-1 Kurokami, Kumamoto 860-8555, Japan. Fax: (096)342-3507, E-mail: tyamao@kumamoto-u.ac.jp*
**(Corresponding author: E-mail: s_atavit@hotmail.com)*

ABSTRACT: To develop a seismic performance evaluation method based on the strain demand control of some critical parts when the arch bridges are subjected to the strong ground motions, it is necessary to establish the method to determine the ultimate strain of each segment (defined as the limit of the strain) which has reached the corresponding critical stress. In this study, the empirical formulas of the ultimate strain corresponding to the failure criterions by in-plane buckling and out-of-plane buckling are investigated and proposed emphasized on the stiffened box-section with longitudinal stiffeners. The applicability of box-cross sections with the longitudinal stiffeners and concrete filled is also been brought into one of the ideas to strengthen the arch bridge where the plasticization are formed in some segments due to the strong ground motion. To perform the analyses, the aspect ratio of the arch member which the lowest maximum strength may be expected was determined beforehand by considering the parameters obtained from linear buckling theory. Then the bending analyses under various axial load ratio parameters were examined to clarify the effect of failure segments in both stiffened sections with and without concrete filled models by the FEM analyses. The post buckling behaviors of concrete filled sections were also observed and compared to the stiffened box-cross sections for each width-to-thickness ratio parameter. Based on the numerical results of the stiffened sections with and without concrete filled models, empirical formulas of the ultimate strain were proposed in functions of width-to-thickness ratio parameter and axial load ratio parameter.

Keywords: Steel arch bridge, performance evaluation, ultimate strain, width-to-thickness ratio parameter, stiffened box-section, concrete filled, post buckling

1. INTRODUCTION

After the 1995 Hyogoken-Nanbu earthquake, the design code recommends that the structures exhibiting complicated seismic behaviors in case of a strong earthquake should be examined based on the results of a dynamic analysis. The two-level ground motion has been proposed for moderate (Level I) and extreme (Level II) ground motions in the earthquake design methodology and the acceptable performance under Level II earthquake has also been established for two objectives which are the safety of the whole structure and the post-earthquake serviceability. This acceptable performance is based on the strain demand control of some critical parts [1]. The dynamic behavior of steel arch bridges can be investigated by one of the simplified methods proposed by dividing the arch ribs and the other members in to beam–column elements and considering each member as a fibered beam element [2]. However, when such members usually composed of thin–walled plates are subjected to the seismic load during a strong earthquake, local buckling of steel members always governs the capacity of the structure. Thus, the effects of local buckling of plate elements in the analysis should also be considered into the design methodology. Furthermore, the equivalent strain over the effective length in each segment at a critical place in failure criterion must be evaluated if the corresponding ultimate strain over the excitation history has been reached. The segment is judged as safe if the average strain time history is always smaller than the ultimate strain in quantity.

To develop a seismic performance evaluation based on response strain index for the arch bridge members, it is necessary to establish the method that is capable to determine the maximum restoring force and the ultimate strain of each segment of the arch ribs. This ultimate strain is defined as the limit of the strain when the steel segments have reached the corresponding critical stress. These sectional strength and strain formula including the effects of interactive local and overall buckling of thin-walled structures can be predicted as a function of the width-to-thickness ratio that is defined by introducing a buckling coefficient based on the elastic buckling analysis [3]. Box-section with a relatively large width-to-thickness ratio was introduced to improve the ductility after buckling behavior in the seismic design. This leads to the improvement of the ductile sections including the use of longitudinal stiffened box- member cross sections. The stiffened box-members have been studied and found to enhance the ductility after buckling behavior if the use of buckling parameters and number of stiffeners are conducted appropriately.

Anyway, to gain high ductility, the large number of stiffeners and uneconomic sizes are required. Moreover, the out-of-plane local buckling caused by the horizontal load is also significant in the ultimate strength of the arch bridge. Thus, the applicability of box-cross section with the longitudinal stiffeners and concrete filled has also been brought into one of the ideas to strengthen the arch bridge where the segments are strongly subjected to high transverse ground motion such as near support locations as shown in Figure 1. However, only few studies have been reported on the ultimate state and local post buckling behavior of the component plates when such a member is subjected to the compressive load and out-of-plane bending moment.

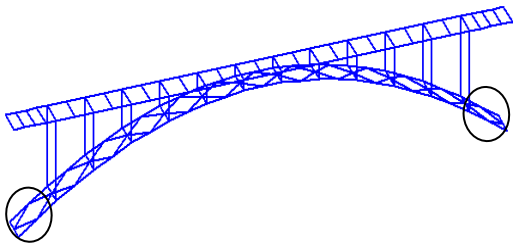

Figure 1. Applied Locations for the Concrete Filled Section

The object of this paper are to propose the empirical formulas of the ultimate strain in order to investigate the failure by in-plane buckling and out-of-plane buckling in frame analyses emphasized on the stiffened box-section with longitudinal stiffeners and to present the post buckling behavior of the box-cross sections with the longitudinal stiffeners and concrete filled following by the empirical formula of the ultimate strain in out-of-plane. To perform the analyses, the aspect ratio representing the diaphragm length of the arch member which the lowest maximum strength may be expected was determined beforehand by considering the parameters obtained from linear buckling theory [4] from the stiffened sections without concrete filled models. Numerical analyses were carried out by the second order elasto-plastic finite element method [7] under the pure compression analysis. Then the bending analyses under various axial load ratio parameters were examined to clarify the effect of failure segments in both stiffened sections with and without concrete filled models. The equivalent section was brought in to the concrete filled models in order to simplify the analyses. The effect of residual stresses and initial crookedness were contemplated and the various buckling parameters which are width-to-thickness ratio and rigidity of stiffeners were also considered. The moment versus rotation angle (M-θ) curves were plotted and compared the differences in ductility after the post buckling behavior while the local buckling failure modes were also observed. Based on the numerical results, empirical formulas to predict the ultimate strain were proposed in a function of the width-to-thickness ratio parameter and axial load ratio parameter.

2. NUMERICAL MODELS AND METHODS

2.1 Stiffened Box-member Cross Sections

A unit length steel arch rib composed of box-profile rectangular cross section member with two or fours stiffeners positioned symmetrically about one axis with respect to member geometry shown in Figure 2 represents the analytical models, Figure 3 shows the cross sectional profile of the box-members. Height, flange width and web width of the analytical models are defined as L_d, F and W respectively. The aspect ratio for the arch rib are defined as $\alpha = (L_d/F)$ and the values of t_f, t_w, b_f and b_w are the thickness of flange, the thickness of web, the width of panel in the flange and the width of panel in the web. In addition t_{sf}, t_{sw}, h_{sf} and h_{sw} represent the thickness of stiffener plates and the height of stiffener plates in flange and web sides, respectively.

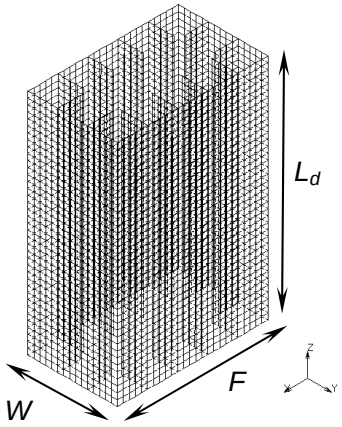

Figure 2. Analytical Model

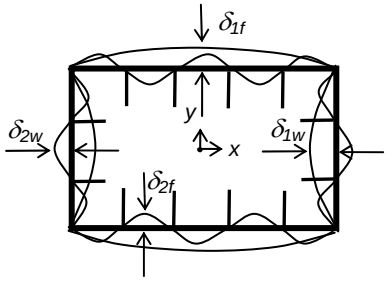

Figure 4. Initial Crookedness of Stiffened Plates

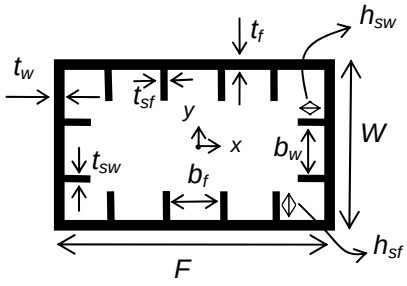

Figure 3. Cross Sectional Profile

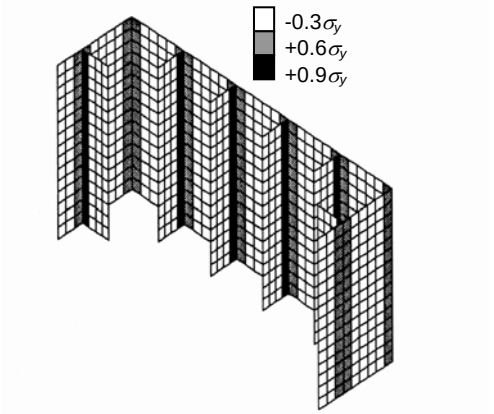

Figure 5. Distribution of Residual Stress

The steel material was assumed to be JIS-SM490 with a yield stress (σ_y) 314 *MPa*, modulus E of 206 *GPa*, and poison's ratio (υ) of 0.3. The initial crookedness of both the panel flange and web plates surrounded by longitudinal stiffeners and the stiffeners were assumed to be a sinusoidal half–wave shape in transverse direction as shown in Figure 4, where its amplitude was assumed to be δ_1 and δ_2 as given in Eq. (1) and Eq. (2) [5]. Residual stresses distributed in trapezoidal pattern in each panel plate were assumed to be $\sigma_{rt} = 0.6\ \sigma_y$, $0.9\sigma_y$ and $\sigma_{rc} = -0.3\sigma_y$ as indicated in Figure 5.

$$\delta_{1f}/\ F = 7.5 \times 10^{-6}\ (F/\ t_f), \quad \delta_{1w}/\ W = 7.5 \times 10^{-6}\ (W/\ t_w) \tag{1}$$

$$\delta_{2f}/\ b_f = 5.0 \times 10^{-5}\ (b_f/\ t_f), \quad \delta_{2f}/\ b_w = 5.0 \times 10^{-5}\ (b_w/\ t_w) \tag{2}$$

The structural parameters obtained from linear buckling theory are described as the followings**;**

The width-to-thickness ratio parameters of the plate panel surrounded by the longitudinal stiffeners for flange and web are defined as R_{rf}, R_{rw} and varied from 0.3 to 0.7 respectively. In this study, the value of R_{rf} was taken to be equal to that of R_{rw} and denoted as R_r. The equations are determined by.

$$R_{rf} = \frac{F}{t_f}\sqrt{\frac{\sigma_y}{E}\frac{12(1-\nu^2)}{k\pi^2}} \tag{3}$$

$$R_{rw} = \frac{W}{t_w}\sqrt{\frac{\sigma_y}{E}\frac{12(1-\nu^2)}{k\pi^2}} \tag{4}$$

Where k is a buckling coefficient (k=4.0n^2, n= number of panels).

The width-to-thickness ratio parameters of the stiffener for flange and web are R_{sf} and R_{sw} and kept to be around 0.7 through all models and denoted as R_s. They are defined by the following equations.

$$R_{sf} = \frac{h_{sf}}{t_{sf}}\sqrt{\frac{\sigma_y}{E}\frac{12(1-\nu^2)}{k\pi^2}} \tag{5}$$

$$R_{sw} = \frac{h_{sw}}{t_{sw}}\sqrt{\frac{\sigma_y}{E}\frac{12(1-\nu^2)}{k\pi^2}} \tag{6}$$

The rigidity of the longitudinal stiffeners compared to a panel plate in the flange side referred to the stiffness ratio of the stiffeners (γ_f / γ_f^*) (γ = relative flexural rigidity of stiffener, γ^* = optimum value of γ obtained from linear buckling theory), are defined by.

$$\gamma_f = \frac{I_{sf}}{Ft_f{}^3/11} \tag{7}$$

$$\left.\begin{aligned} \gamma_f{}^* &= 4\alpha_f{}^2 n(1+n\delta_1) - \frac{(\alpha_f{}^2+1)^2}{n}, \qquad t_f < t_o,\ \alpha \le \alpha_o \\ \gamma_f{}^* &= 4\alpha_f{}^2 n(1+n\delta_1)\left(\frac{t_o}{t_f}\right)^2 \frac{(\alpha_f{}^2+1)^2}{n}, \quad t_f \ge t_o,\ \alpha \le \alpha_o \end{aligned}\right\} \tag{8}$$

Where I_{sf} is the moment of inertia of each stiffener about the base axis

α_f is the aspect ratio compared to the flange side and can be obtained from L_d / F
L_d is the diaphragm spacing in the arch member
n is number of panels in the flange side
$t_o = F / (24fn)$
f=1 for pure compression or compression through bending.
$\delta_1 = A_{sf} / Ft_f$, where A_{sf} is the cross sectional area of a stiffener
α_{of} is the limitation of an aspect ratio in the flange side and can be obtained from

$$\alpha_o = \sqrt[4]{1+n\gamma} \tag{9}$$

The stiffener's slenderness ratio parameter [6] in the flange side, $\bar{\lambda}_{sf}$ is given by

$$\bar{\lambda}_{sf} = \frac{1}{\sqrt{Q}} \frac{L_d}{r_s} \frac{1}{\pi} \sqrt{\frac{\sigma_y}{E}} \tag{10}$$

Where Q is the local buckling strength of the sub-panel plate and defined by

$$Q = \frac{1}{2R_{rf}} \left[\beta - \sqrt{\beta^2 - 4R_{rf}} \right] \leq 1 \tag{11}$$

$$\beta = 1.33R_{rf} + 0.868 \tag{12}$$

r_s is the radius of gyration of the T- cross section consisting of one longitudinal stiffener and the adjacent sub-panel of width F/n

The rigidity of the longitudinal stiffeners compared to a panel plate (γ_w / γ_w^*) and the stiffener's slenderness ratio parameter (λ_{sw}) in the web side can also be obtained from the similar equations calculated for the flange side.

The analyses were carried out by using the FEM package program [7] on the full section of members along the unit length and simply supported boundary conditions were applied in all cases. The elasto-plastic large displacement analyses were performed and a plate element type of four-node quad was applied. The stress-strain curve used in these analyses was assumed to be multi-linear where strain hardening first occurs at the strain ε_{st}, 7 times of the yield strain ε_y and the hardening modulus E_{st} is $E/30$ as shown in Figure 6.

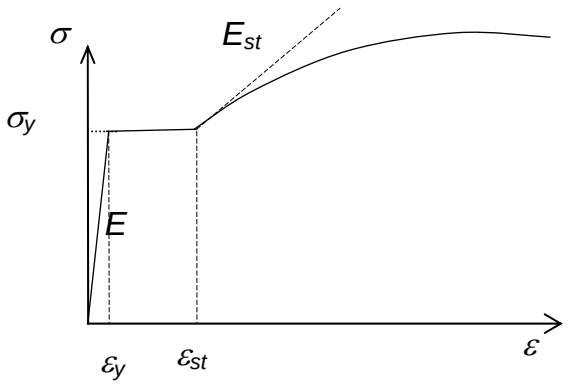

Figure 6. Multi-linear Stress-strain Relationship

2.2 Aspect Ratio of the Arch Member obtained from the Pure Compression Analysis

Rectangular cross section 1500 mm x 900 mm was chosen to determine the aspect ratio of the arch rib which the lowest maximum strength is expected under the pure compression analysis by using the displacement control as shown in Figure 7. By considering the parameters obtained from linear buckling theory as mentioned above, six values of the aspect ratio of the stiffened plate in the flange side (α_f) applied for the real arch bridges were chosen to be 1.0, 1.1, 1.2, 1.3, 1.4 and 1.5 and represented to be A, B, C, D, E, and F models, respectively. The width–to-thickness ratio parameters of the plate panel surrounded by the longitudinal stiffeners for flange and web (R_{rf} and R_{rw}) were ranged from 0.3 to 0.7. The width–to-thickness ratio parameters of the stiffener for web

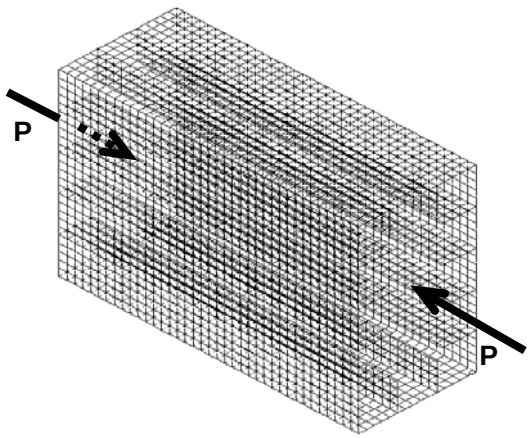

Figure 7. Pure Compression Analysis Model

and flange (R_{sf} and R_{sw}) were fixed to be 0.7 and the stiffness ratio of the stiffeners in both flange and web panels (γ / γ^*) was also kept to be 3.0 constantly. Table 1 shows the geometries and structural parameters obtained from linear buckling theory for these models. Figure 8 shows the plots between the equivalent strength ratio σ / σ_y versus the equivalent strain ratio $\varepsilon / \varepsilon_y$ for the values analyzed from F models. The optimum aspect ratio in the arch member could be obtained by considering the minimum ultimate strength ratio versus R_r values in Figure 9 where the value of α equal to1.5 (F model) gave the lowest ultimate strength ratio in all cases

Table 1. Geometries and Structural Parameters used in Pure Compression Analysis

No.	Model types	Structural parameters						Flange side (mm)				Web side (mm)			
		R_s	γ/γ^*	α_f	α_{of}	α_{ow}	R_r	F	t_f	h_{sf}	t_{sf}	W	t_w	h_{sw}	t_{sw}
1	A03	0.7	3.0	1.0	3.54	3.30	0.3	1500	20.5	187.3	16.8	900	20.5	174.6	15.7
2	A05				4.73	4.64	0.5		12.3	171.0	15.4		12.3	167.6	15.1
3	A07				4.64	4.54	0.7		8.8	130.0	11.7		8.8	127.3	11.5
4	B03			1.1	3.76	3.47	0.3		20.5	198.6	17.9		20.5	183.4	16.5
5	B05				5.03	4.92	0.5		12.3	181.8	16.4		12.3	177.7	16.0
6	B07				4.92	4.80	0.7		8.8	137.9	12.4		8.8	134.7	12.1
7	C03			1.2	3.96	3.62	0.3		20.5	209.6	18.6		20.5	191.6	17.2
8	C05				5.33	5.19	0.5		12.3	192.4	17.3		12.3	187.6	16.9
9	C07				5.19	5.06	0.7		8.8	145.7	13.1		8.8	141.9	12.8
10	D03			1.3	4.17	3.77	0.3		20.5	220.4	19.8		20.5	199.1	17.9
11	D05				5.61	5.46	0.5		12.3	202.9	18.3		12.3	197.4	17.6
12	D07				5.47	5.31	0.7		8.8	153.3	13.8		8.8	149.0	13.4
13	E03			1.4	4.37	3.90	0.3		20.5	231.0	20.8		20.5	206.0	18.5
14	E05				5.90	5.73	0.5		12.3	213.3	19.2		12.3	207.0	18.6
15	E07				5.74	5.55	0.7		8.8	160.9	14.5		8.8	155.8	14.0
16	F03			1.5	4.56	4.01	0.3		20.5	241.4	21.7		20.5	212.1	19.1
17	F05				6.19	5.99	0.5		12.3	223.5	20.1		12.3	216.5	19.5
18	F07				6.00	5.79	0.7		8.8	168.3	15.2		8.8	162.5	14.6

2.3 Concrete Filled Sections

The concrete filled box sections with longitudinal stiffeners were further investigated by focusing on the F model (α = 1.5) which the lowest maximum strength had been obtained. In order to validate the analytical results and to understand their behavior gradually, the five values of R_r ranged from 0.3 to 0.7 increasing in 0.1 steps would be analyzed and represented by CF03 to CF07 models respectively. The equivalent section concept was brought to transform the original stiffened section to the equivalent section by preserving the constant sectional area A, and plastic section modulus Z [8]. The original and equivalent sections are shown in Figure 10. Flange and web widths of transformed section were kept to be constant as same as the original one. Equivalent flange and web thicknesses are defined as $\bar{t}_f$ and $\bar{t}_w$ respectively, and the equivalent sectional area can be calculated by Eq. (13) to Eq. (15).

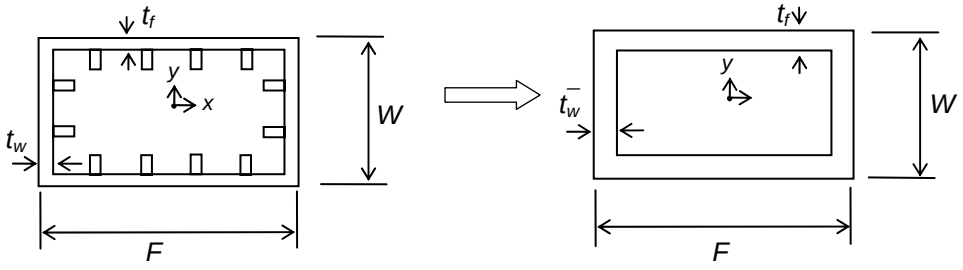

(a) Original Section (b) Equivalent Section

Figure 10. Transformation of Concrete Filled Box-section

$$A = 2\left[F\bar{t}_f + \left(W - 2\bar{t}_f\right)\bar{t}_w\right] \tag{13}$$

$$\bar{t}_f = \frac{4Z - AW}{2(FW - A)} \tag{14}$$

$$\bar{t}_w = \frac{A - 2F\bar{t}_f}{2(W - 2\bar{t}_f)} \tag{15}$$

Note that Z is the plastic section modulus about the x axis.

The plastic moment about the x-axis, M_p is also defined by Eq. (16)

$$M_p = F\bar{t}_f(W - \bar{t}_f)\sigma_{yf} + \frac{1}{2}(W - 2\bar{t}_f)^2\bar{t}_w\sigma_{yw} \tag{16}$$

Which σ_{yf} and σ_{yw} represent the yield stress of the steel, σ_y.

The structural, geometrical and sectional properties of the original and equivalent sections of F models are shown in Table 2. For the concrete material's properties, the Young's modulus (E) was assumed to be 24.5 *GPa*, compressive strength (σ_c) 23.5 *MPa* and poison's ratio (υ) of 0.20, respectively. The same residual stresses distributed in trapezoidal pattern applied to the stiffened box-sections were treated. The initial crookedness shown in Figure 11 was assumed to be a cosine half–wave where its amplitude was assumed to be F/150 and W/150 in flange and web panels, respectively.

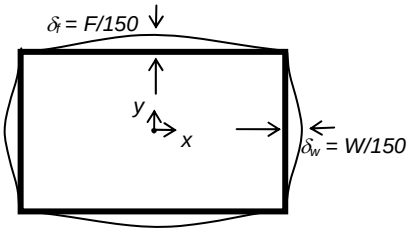

Figure 11. Cosine Half-wave Initial Crookedness

Table 2. Structural, Geometrical and Sectional Properties of CF Models

No	Model Types	Structural parameters			Original geometries (mm)					Transformed Geometries (mm)		Sectional properties	
		Rr	λsf	λsw	tf, tw	hsf	tsf	hsw	tsw	$\bar{t}_f$	$\bar{t}_w$	A (mm2) X102	Z (mm3) X103
1	CF03	0.3	0.3435	0.4072	20.5	241.4	21.7	212.1	19.1	25.3	46.5	1549	49965
2	CF04	0.4	0.3303	0.3549	15.4	232.7	20.9	220.2	19.8	19.8	40.6	1293	41213
3	CF05	0.5	0.3366	0.3506	12.3	223.5	20.1	216.5	19.5	16.6	35.5	1114	35359
4	CF06	0.6	0.4035	0.4214	10.3	191.6	17.2	185.2	16.7	14.1	26.1	876	28597
5	CF07	0.7	0.4741	0.4957	8.8	168.3	15.2	162.5	14.6	12.1	20.3	718	23884

3. BENDING ANALYSIS UNDER AXIAL COMPRESSION

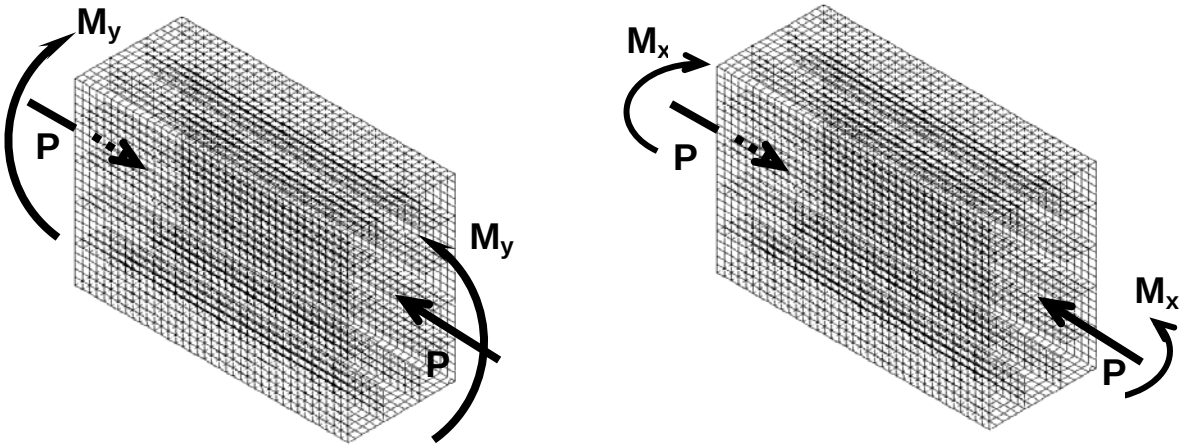

(a) In-plane Bending Moment (b) Out-of-plane Bending Moment

Figure 12. Bending Analytical Models under Axial Compression

These analyses were performed in two stages, initially, the F models of stiffened box cross-sections would be investigated the ultimate state of the stub column subjected to the in-plane and out-of-plane bending moment (about y and x-axes in this case) by using the rotation control under various ratios of compressive load. Latterly, the F models of the equivalent stiffened ones with concrete filled would be further examined by emphasizing on the ultimate state of the stub column subjected to the out-of-plane bending moment by using the same method mentioned previously. The analytical models under the compressive loads subjected to in-plane and out-of-plane bending moments are shown in Figures 12(a) and 12(b), respectively. In all analyses, both bending moment and compressive load were applied to only on the steel section through the top and bottom rigid plates and the concrete elements were merely allowed to prevent the failure from the concave local buckling of the component plates. In order to investigate the effect of axial load on the ultimate moment and ultimate strain, the load ratios P/P_y, were ranged from 0 to 0.8, where P_y represents the yield compressive strength obtained from the elastic theory. For the concrete filled model analyses, the same numerical analyses and boundary conditions applied for the stiffened box-cross section were applied to the steel in these equivalent sections. A type of eight-node hex solid element was applied to concrete elements and the contact bodies analysis was applied to constrain the nodes on the exterior surfaces in both steel and concrete elements not to penetrate to each other including their own bodies.

4. RESULTS AND DISCUSSIONS

4.1 Stiffened Box Cross-section Models

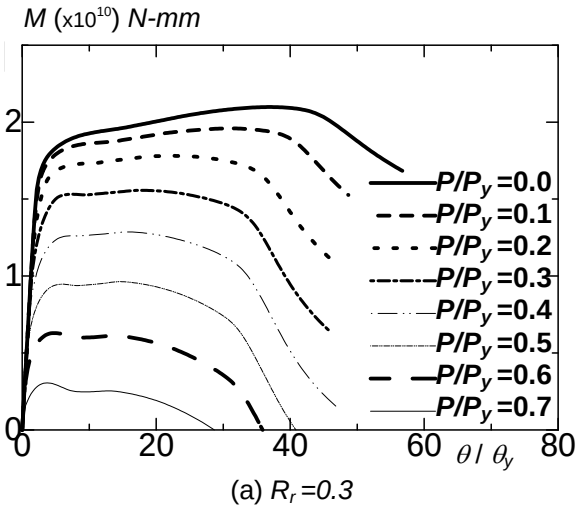

(a) R_r =0.3

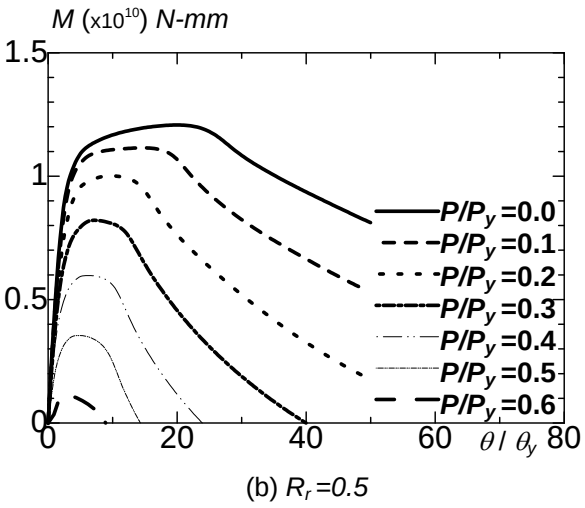

(b) R_r =0.5

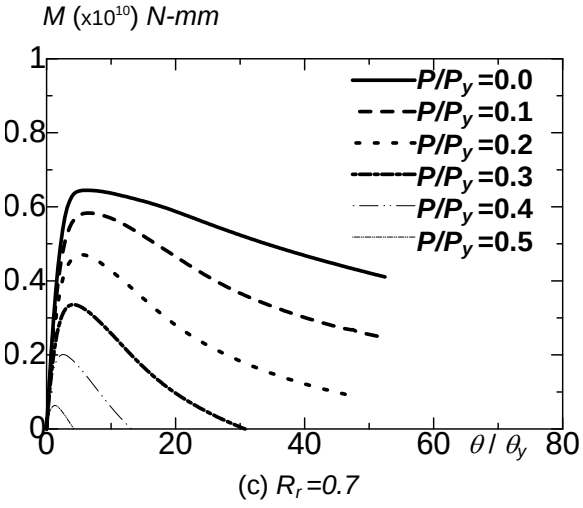

(c) R_r =0.7

Figure 13. Results obtained from In-plane Bending Analyses

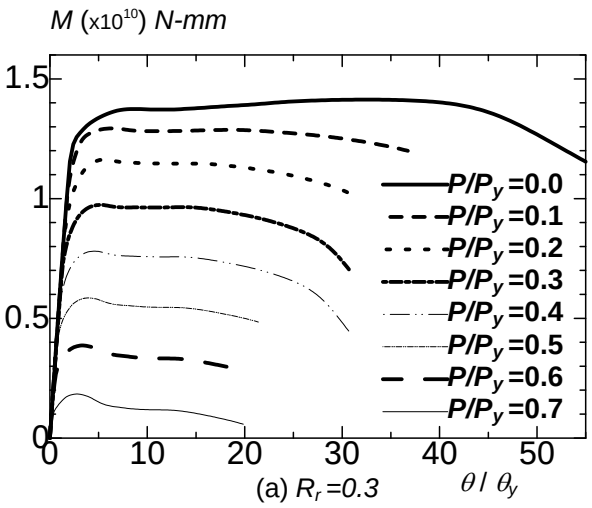

(a) R_r =0.3

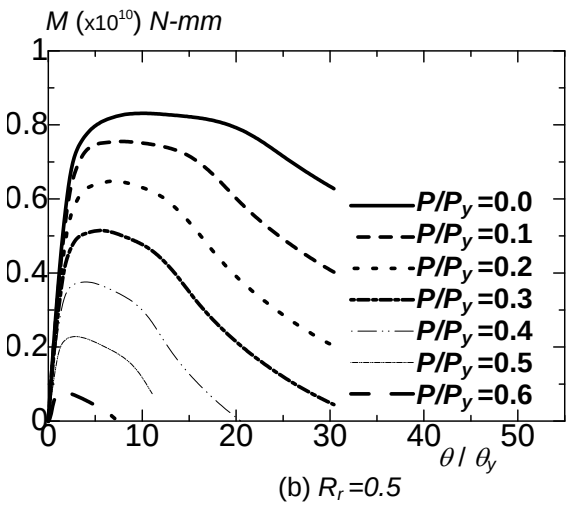

(b) R_r =0.5

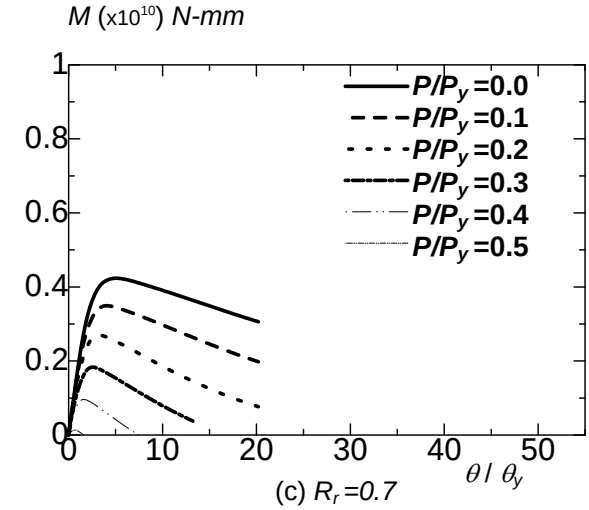

(c) R_r =0.7

Figure 14. Results obtained from Out-of-plane

The analytical results would be plotted between the reaction moment M versus the applied rotation angle ratio θ / θ_y, where θ_y refers to the yield rotation angle which induces the axial yield strain ε_y. Figures 13(a), 13(b), 13(c) show the analytical results obtained from the in-plane bending analyses of the stiffened box cross-sections while Figures 14 (a), 14 (b) and 14 (c) are taken from the out-of-plane. Both results from in-plane and out-of-plane analyses clearly showed the similar phenomenon. It was found that for the same value of R_r, the reaction moment tended to decrease when the load ratio increased. When R_r equals to 0.5 and 0.7, the moment values were found to decrease more rapidly than when R_r equals to 0.3 for the same ratio of axial load in the large amount of rotation after the local buckling of the component plates had occurred. Numerical analyses of the load ratios over than 0.7 in model $R_r = 0.3$, 0.6 in model $R_r = 0.5$ and 0.5 in model $R_r = 0.7$ could not be achieved because the severe local buckling occurred in the early stage of the analyses and the calculations could not be longer performed. The results suggested that the effects of the axial load ratio and the structural parameter R_r on the ultimate strength of the member considered as a stub column were large. The analytical results also indicate that the reaction maximum moments obtained from the in-plane bending analyses were larger than the out-of-plane's results in any cases of the R_r and the axial load values. In order to consider the ultimate state of stub columns, the plots of ultimate moment M_u versus R_r and the plots of ultimate strain ratio $\varepsilon_u/\varepsilon_y$ versus the product of structural parameters $R_r(\ \bar{\lambda}_{sf}\ \ \bar{\lambda}_{sw})^{\ 0.09}$ were considered, where M_u is defined as the moment corresponding to 95 % of the maximum moment after the peak region and ε_u refers to the strain corresponding to M_u at the outmost edge of the compressive side. The ultimate moment values are shown in Figure 15(a), 15(b) and the ultimate strain ratios are shown in Figure 16(a) and Figure 16(b) while (a) and (b) represent the results obtained from in-plane and out-of-plane analyses respectively. It was obviously recognized that the ultimate moment decreased when the load ratio increased for all values of R_r. The slightly difference in the ultimate moment compared to the result obtained from the next value of load ratio were found when the load ratios were small and these differences in the ultimate moment tended to increase when the load ratios were larger.

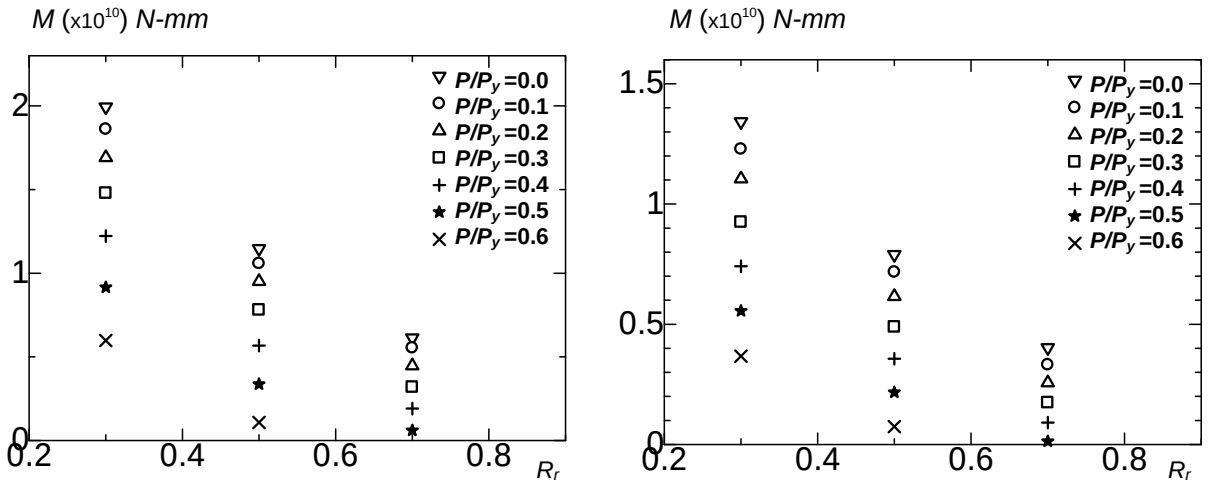

(a) In-plane Analyses (b) Out-of-plane Analyses

Figure 15. The Ultimate Moment Values at the Ultimate State

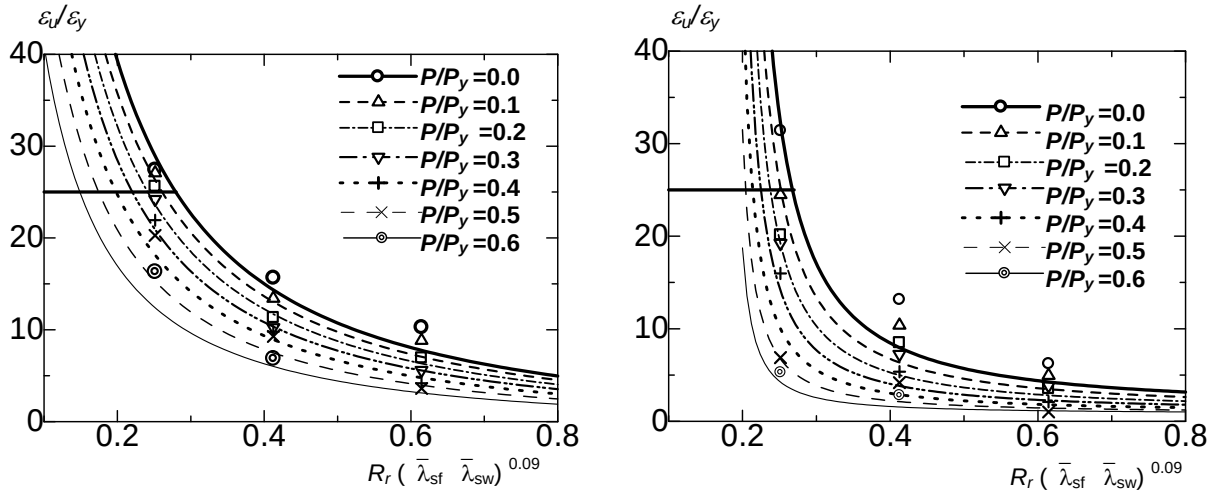

(a) In-plane Analyses (b) Out-of-plane Analyses

Figure 16**.** The Ultimate Strain Ratios at the Ultimate State

By considering the results in Figure 16(a) and Figure 16(b), the strain ratios obtained from in-plane analyses were mostly found slightly higher than the ones obtained from out-of-plane analyses for the same values of the structural parameters and the axial load ratio. The design formulas obtained from the least square method of the ultimate strains judged from the safety of the whole segments in both in-plane and out-of-plane can be proposed by the following equations.

In-plane, $$\varepsilon_u / \varepsilon_y = \frac{4.9}{\left(R_r\left(\bar{\lambda}_{sf}\,\bar{\lambda}_{sw}\right)^{0.09} - 0.16\right)^{1.4}\left(1 - P/P_y\right)^{0.9}} - \frac{1.5}{\left(1 + P/P_y\right)} \le 25 \quad (17)$$

Out-of-plane, $$\varepsilon_u / \varepsilon_y = \frac{1}{\left(R_r\left(\bar{\lambda}_{sf}\,\bar{\lambda}_{sw}\right)^{0.09} - 0.18\right)^{1.3}\left(1 - P/P_y\right)^{2.4}} + \frac{1.3}{\left(1 + P/P_y\right)} \le 25 \quad (18)$$

When $0.3 \le R_r \le 0.7$ and $0 \le P/P_y \le 0.6$

4.2 Equivalent Stiffened Box Cross-section Models with Concrete Filled

Figure 17(a) to Figure 17(e) show the analytical results obtained from the out-of-plane bending analyses of the equivalent stiffened box cross-section models with concrete filled. It can be noted that the concrete filled models can develop the out-of-plane ultimate moment at the ultimate state compared to the results obtained from the stiffened box cross-section models and the greater values were found where the width-to-thickness ratio parameters and the axial load ratios were small. To obtain the ultimate state of the members, the same method used previously was applied by considering the plots of ultimate moment and ultimate strain ratio as shown in Figure 18 and Figure 19. Because of the difference and complexity of the post buckling modes occurred due to the different values of R_r and the axial load values, the moment corresponding to 97% of the maximum moment after the peak region was determined to represent the ultimate moment, M_u and the ultimate strain, ε_u still refers to the strain corresponding to M_u . In order to clearly understand the behavior during the ultimate state, the post buckling behaviors and mode shapes observed in steel plates during the ultimate state and the failure of concrete characteristics will be described in next topic.

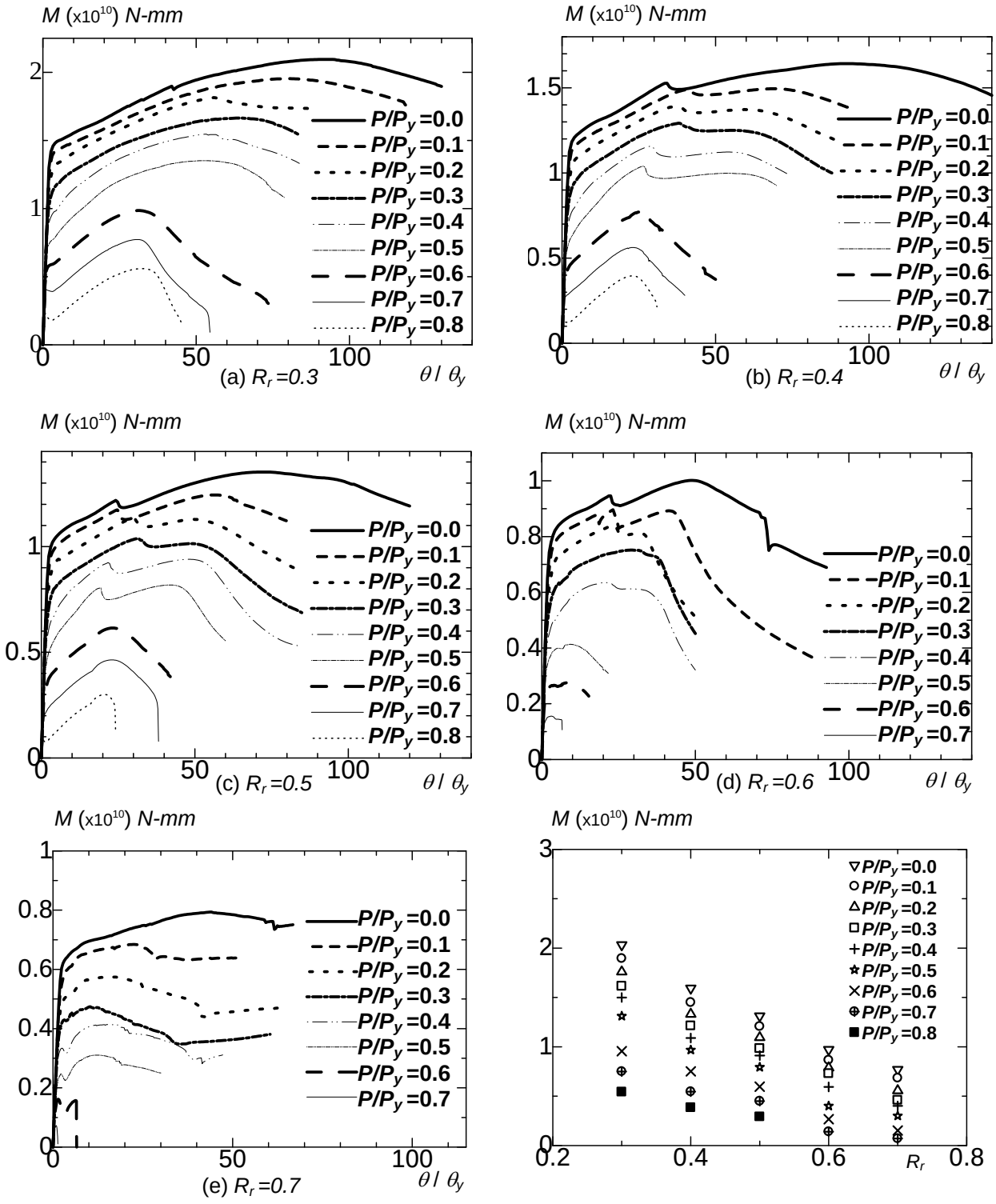

Figure 17. Results obtained from Equivalent Stiffened Box -section with Concrete Filled Models

Figure 18. The Ultimate Moment Values

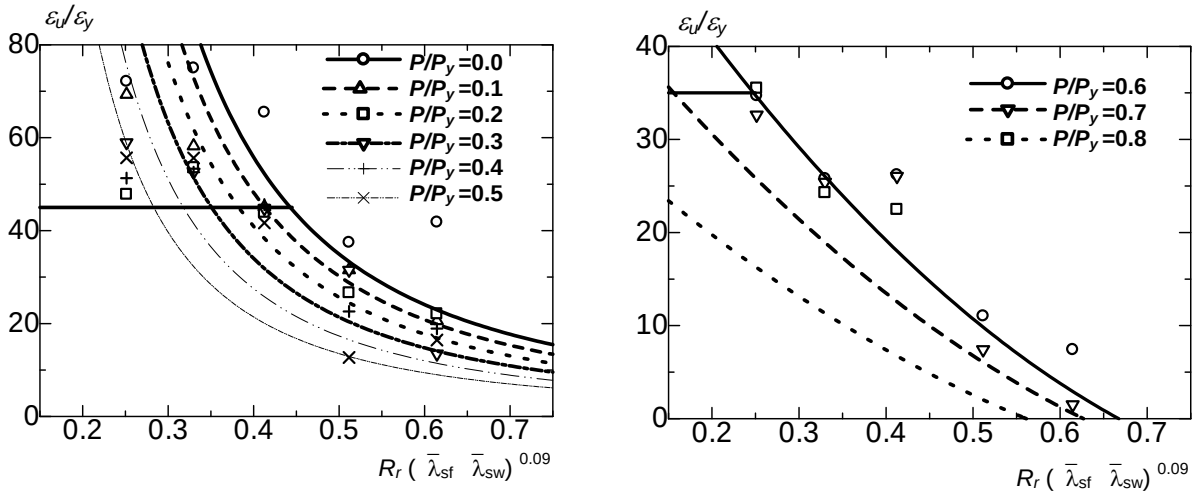

(a) $0.0 \le P/P_y \le 0.5$ (b) $0.6 \le P/P_y \le 0.8$

Figure 19**.** The Ultimate Strain Values obtained from Concrete Filled Models

Because the local buckling modes observed when the axial load ratios are higher than 0.5 differed from the others, the ultimate strain values will also be considered separately as shown in Figure 19(a) and Figure 19(b) respectively. Once again, the empirical formula obtained from the least square method of the ultimate strain for the equivalent stiffened box cross-section models with concrete filled in out-of-plane can be proposed by the following equations.

$$\varepsilon_u / \varepsilon_y = \frac{7.5}{\left(R_r\left(\bar{\lambda}_{sf}\,\bar{\lambda}_{sw}\right)^{0.09} - 0.03\right)^2 \left(1 - P/P_y\right)^{1.4}} + \frac{1}{\left(1 + P/P_y\right)} \le 45 \tag{19}$$

When $0.3 \le R_r \le 0.7$ and $0 \le P/P_y \le 0.5$

$$\varepsilon_u / \varepsilon_y = 160(R_r(\bar{\lambda}_{sf}\,\bar{\lambda}_{sw})^{0.09} - 1)^2 (1 - P/P_y)^{0.8}) - 8.5 \le 35 \tag{20}$$

When $0.3 \le R_r \le 0.7$ and $0.6 \le P/P_y \le 0.8$

4.3 Post Buckling Behavior of Stiffened Box Cross-section Models with Concrete Filled

Finally, the post buckling behavior of the concrete filled models will be investigated by the comparison of the moment ratio M / M_p versus the rotation angle ratio θ / θ_y plots between the out-of-plane's numerical results obtained from stiffened box sectional models (F) and concrete-filled models (CF) for R_r = 0.3 and 0.5 as shown in Figures 20(a) and 20(b), respectively. The relations show that after the buckling occurs, the increasing of moment ratio in the large rotation applied region is observed for each concrete filled model and it can be implied that the use of concrete with stiffeners in arch member box-section can improve the member's ductility in the post buckling state. In order to discuss the development in ultimate moment and ductility phenomena, two observations are suggested in the following comments.

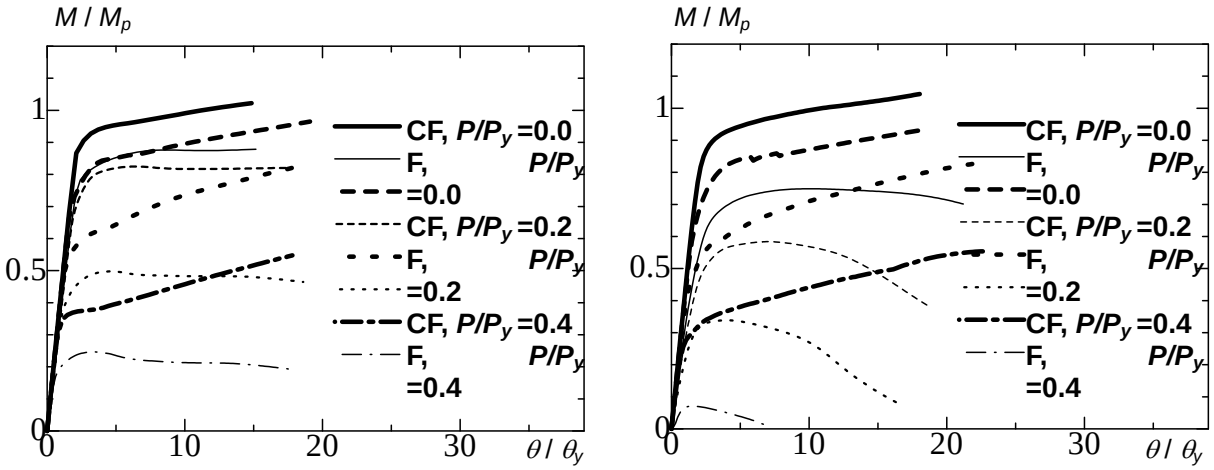

(a) $R_r = 0.3$ (b) $R_r = 0.5$

Figure 20. Comparisons between Stiffened Box Sectional Models and Concrete Filled Models

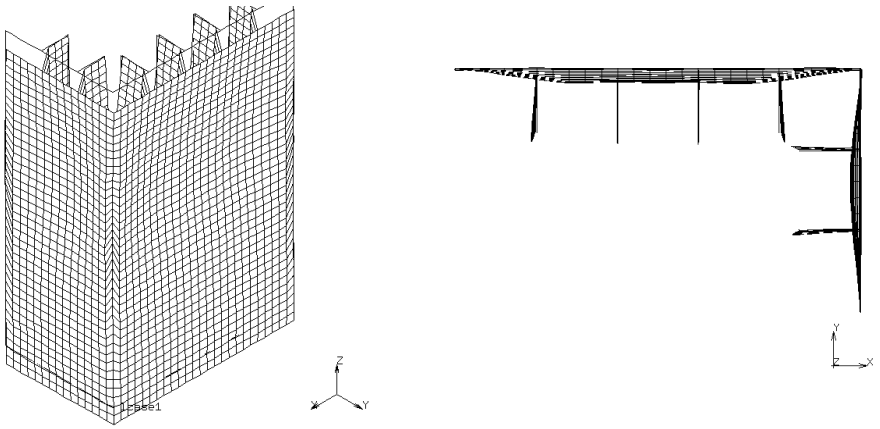

(a) 3-D View (b) Top View

Figure 21. Typical Local Buckling Mode Shape Found in Stiffened Box Sectional Models

The local buckling modes during the ultimate state were observed and found that in the stiffened box sectional models, the inward buckling occurred in both the surrounding plates and stiffeners as shown in Figures 21 followed by the failure of the whole structure, while in concrete filled models, the outward buckling was found in web and flange panels subjected to the compressive flexural stress. Three different types of buckling shape shown in Figure 22 (a) to Figure 22 (c) were found in different width-to-thickness ratio parameters, R_r and the values of axial load ratio P/P_y. The secondary local buckling mode shapes similar to Figure 22(a) was found in models CF03, CF04, CF05 and CF06 when the values of load ratio are smaller than 0.6 and the one similar to Figure 22 (b) was found in models CF07, respectively. When the axial load ratios being higher than 0.5, the single local buckling mode similar to Figure 22 (c) was formed in every CF models. The stress concentration in concrete commenced from both middle corners of the concrete height in the compressive side and expanded over the local buckling effective length during the ultimate state. The intense stress concentration was particularly found in the middle zone coincidently where the component plate in the middle flange had buckled and the stress intensity was mostly found higher than the compressive strength of concrete material. The stress concentration generated from the tension side was similar to the compressive side but less intensity. It can be suggested that in concrete filled box-section models, the mode shapes when the component plates buckled are influenced by the structural parameter R_r, and the compressive load ratio, P/P_y. Due to the inward

buckling prevention of concrete in core, the members could sustain the load and bending moment after the local buckling had occurred and then revealed the ductility behavior of the members

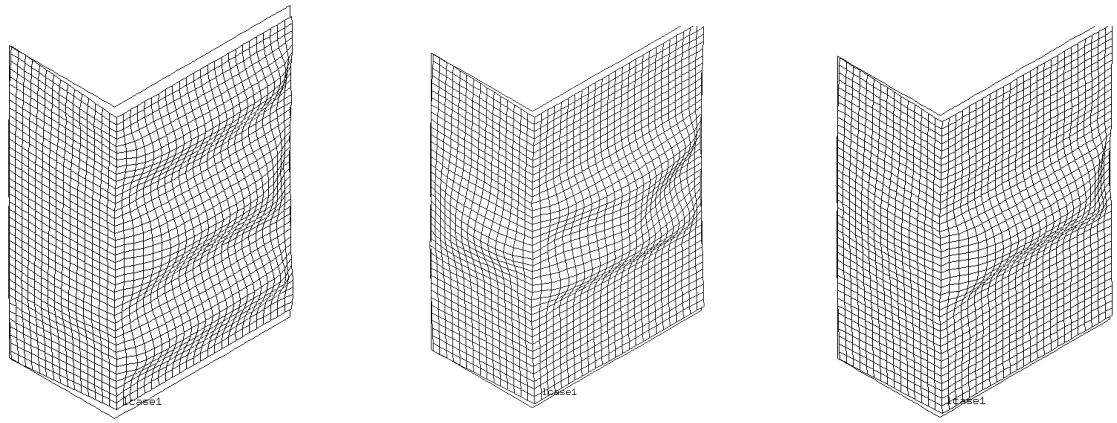

(a) In Models CF03-CF06 (b) In Models CF07 (c) When $P/P_y > 0.5$

Figure 22. Local Buckling Modes Observed in Concrete Filled Models

Horizontal displacements at the center in y-direction of the flange plates subjected to the compressive flexural stress were continually investigated in order to clarify the effect of the buckling mode shapes to the failure behaviors when the component plates have buckled. Figures 23 shows the comparison between the horizontal displacements in y-direction taken from the models R_r = 0.5 versus analytical increment steps. The left portion represents the results obtained from concrete filled box-section models (CF) while stiffened box-cross section' ones (F)are shown in the right side.

From Figure 23, it can be apparently noticed that in CF models, when the load ratios are less than 0.6, the incremental displacements in Y-direction increase differently compared to when the load ratios are over than 0.6 and can be separated in two main stages. The rapid increasing in horizontal displacements was formed in the earlier steps of the analyses following by the sudden shift when the displacements had reached the values approximately 120 to 150 mm and continued until the last analytical steps. In the latter stage, only slightly decreasing in displacements was also observed in some cases. This plot's characteristic refers that in the earlier stage of the load applied, the single local buckling mode is formed in the middle part of the component plate until a specific value of the horizontal displacement has been reached. After that, the secondary buckling will gently take place in the top and bottom portions until the member reaches its ultimate state and continue performing thorough the failure stage. On the other hand, the results found in the other CF models including results obtained from the F models indicate that only the single buckling mode was formed since the plate had buckled until the component plate had attained its ultimate horizontal displacement. Regarding to the result obtained from the F model of the load ratio equals 0.8, the abrupt

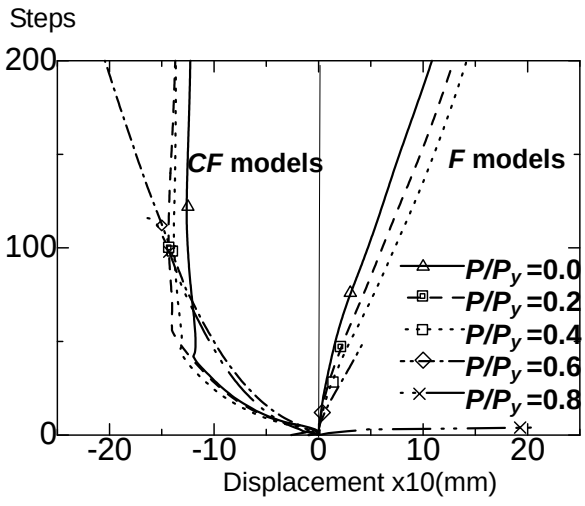

Figure 23. Horizontal Displacements at the Mid-height Point taken from Models R_r = 0.5

failure is noticeable due to the infinite displacement in the earlier stage of the applied load. Horizontal displacements measured at the ultimate state of the F and CF models are coincident with the post buckling behavior during the ultimate state. The horizontal displacements measured in CF models have slightly differences among them but largely differ from the results obtained from the F models. The mark symbols in Figure 23 identify the positions corresponding to when the ultimate states have been reached and these horizontal displacements at the ultimate states are plotted versus the axial load ratio parameters and compared in Figure 24. Results obtained for the F models (represented by the solid circles) show that when there is no compressive load applied, $P/P_y = 0$, only small horizontal ultimate displacements were found and these displacements would slightly decrease when the load ratio increased. In CF models, the large amount in horizontal displacements was found and slightly differences were observed when the axial load ratio parameters were varied. When the load ratios are less than 0.6, note that the ultimate horizontal displacements were all found during the secondary buckling modes had been being formed. Due to the large amount in horizontal displacements and local buckling modes, the concrete filled models could attain the higher ultimate moment than those obtained form the stiffened box cross-section ones.

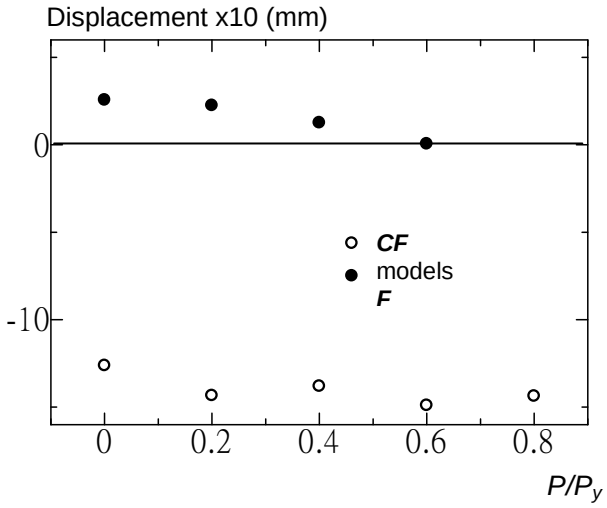

Figure 24. Horizontal Displacements Measured at the Ultimate State

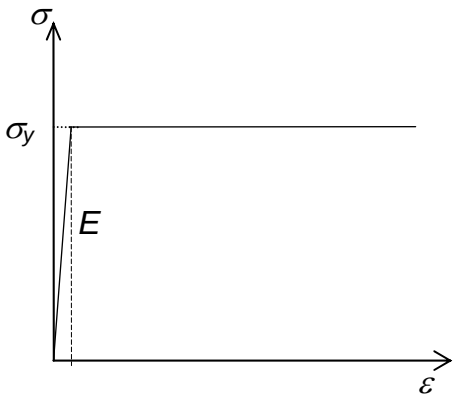

Figure 25. Bi-linear Stress-strain Relationship

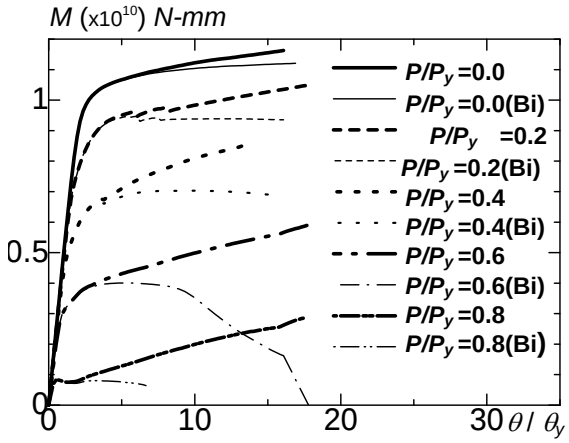

Figure 26. Effect of Strain Hardening in Multi-linear Stress-strain Relationship

Another suggestion was made by the consideration in material's properties. Bi-linear stress-strain curve as shown in Figure 25 was input into the analyses to compare the effect of the strain hardening during the post buckling state in the component steel plates. The analyses were conducted and compared to the analytical results obtained when the multi-linear stress-strain relationship was applied for the models R_r = 0.5. These comparisons are plotted and shown in Figure 26. The reaction moment results obtained when the bi-linear stress-strain relationship was considered in the analyses are represented by the thin lines. It is clearly understood from the figure that the effect of strain hardening in steel material are dominant after the local buckling behavior. The numerical results indicated that the use of concrete with stiffeners in arch member box-section can improve the member's ductility in the post buckling state.

5. CONCLUSIONS

The unit length of steel arch bridge box-members composed of stiffeners in flange and web panels were investigated to obtain the formulas which can determine the ultimate strain of each segment of the arch ribs respect to in-plane and out-of-plane of the arch. The application of concrete-filled was also considered to improve the ultimate strength and ductility of the members thus, the equivalent stiffened box cross-section with concrete filled models were introduced into the analyses. From the numerical results obtained, the main conclusions of this study are summarized as the followings.

1) The aspect ratio of the arch bridge member with the cross section 1500x900 mm obtained from the pure compression test is determined to be 1.5.

2) From the numerical results obtained from stiffened box-member cross sections and equivalent stiffened box cross-section with concrete filled models subjected to bending moment under various compressive loads, it is found that the ultimate moment ratio tends to decrease when the load ratio increases for the same value of width-to-thickness ratio parameters, R_r.

3) The ultimate state of the box members subjected to bending analysis under compressive load is considered by the ultimate moment ratio and ultimate strain ratio and the latter can be proposed as functions of the axial load parameter P/P_y and the width-to-thickness ratio parameter.

4) In concrete filled box-section models, the mode shapes when the component plates have buckled are influenced by the structural parameter R_r, and the compressive load ratio, P/P_y.

5) By the equivalent section applied concept, the numerical results obtained from the FEM analysis show that the use of concrete filled stiffened box-section in arch members can improve the ultimate strength and ductility in the post buckling stage because of the influences of the difference in local buckling failure mode shapes and the effect of the strain hardening in steel material.

REFERENCES

[1] Usami, T. Lu, Z. Ge, H.B. and Kono, T., “Seismic Performance Evaluation of Steel Arch Bridges Against Major Earthquakes. Part 1: Dynamic Analysis Approach”, Earthquake Engng. Struct. Dyn., 2004, pp. 1337-1354.

[2] Sakimoto, T., Watanabe, H., Tsuchida, S. and Miwa, K., “A Simplified Analysis of Steel Frames Fail by Local and Global Instability”, Proc. of the 5th International Colloquium on Stability and Ductility of Steel Structures, 1977, Vol. 2, pp. 777-784.

[3] Zheng, Y., Usami, T., Ge, H.B., “Ductility Evaluation Procedure for Thin-walled Steel Structure”, Journal of Structural Engineering, ASCE, 2000, Vol. 126, pp.1312-1319.

[4] “Design Specifications for Highway Bridges”, Part II Steel Bridge and Part V Seismic Design, Japan Road Association, 2002. (In Japanese)

[5] Komatsu, S. Ushio, M. and Kitada, T., “An Experimental Study on Residual Stresses and Initial Deformations of Stiffened Plates”, Proceedings, JSCE, 1997, pp. 25-35. (In Japanese)

[6] Zheng, Y., Usami, T., Ge, H.B., “Ductility of Thin-walled Steel Box Stub-columns”, Journal of Structural Engineering, ASCE, 2000, Vol. 126, pp. 1304-1311.

[7] “MARC K7 User Manual”, A-E., NIPPON MARC, 2001.

[8] Usami, T., Suzuki, M., Iraj, H.P. Mamaghani and Ge, H.B.., “A Proposal for Check of Ultimate Earthquake Resistance of Partially Concrete Filled Steel Bridge Piers”, Journal of Structural Mechanics and Earthquake Engineering, 1995, Vol. 353, No. 525, pp. 69-82. (In Japanese)

[9] Zhanfei, W. Yamao, T. Ishii, Z. and Iwatsubo, K., “Applicability of Static-dynamic Verification Method for Seismic Design of Bridge Piers with Inner Cruciform Walls”, Proceedings ICSCS’04, 2004, pp. 789-798.

[10] Mohamed, O., Sakimoto, T. and Yamao, T., “Ductility of Stiffened Plates after Buckling as a Component of a Box Cross-section”, Proceedings ICSCS’04, 2004, pp. 299-308.